Quantification of Extracellular Carbonic Anhydrase Activity in Two Marine Diatoms and Investigation of Its Role[1][W][OA]

Brian M. Hopkinson*, Christof Meile, and Chen Shen

Department of Marine Sciences, University of Georgia, Athens, Georgia 30602

Many microalgae induce an extracellular carbonic anhydrase (eCA), associated with the cell surface, at low carbon dioxide (CO_2) concentrations. This enzyme is thought to aid inorganic carbon uptake by generating CO_2 at the cell surface, but alternative roles have been proposed. We developed a new approach to quantify eCA activity in which a reaction-diffusion model is fit to data on ^{18}O removal from inorganic carbon. In contrast to previous methods, eCA activity is treated as a surface process, allowing the effects of eCA on cell boundary-layer chemistry to be assessed. Using this approach, we measured eCA activity in two marine diatoms (*Thalassiosira pseudonana* and *Thalassiosira weissflogii*), characterized the kinetics of this enzyme, and studied its regulation as a function of culture pH and CO_2 concentration. In support of a role for eCA in CO_2 supply, eCA activity specifically responded to low CO_2 rather than to changes in pH or HCO_3^-, and the rates of eCA activity are nearly optimal for maintaining cell surface CO_2 concentrations near those in the bulk solution. Although the CO_2 gradients abolished by eCA are small (less than 0.5 μM concentration difference between bulk and cell surface), CO_2 uptake in these diatoms is a passive process driven by small concentration gradients. Analysis of the effects of short-term and long-term eCA inhibition on photosynthesis and growth indicates that eCA provides a small energetic benefit by reducing the surface-to-bulk CO_2 gradient. Alternative roles for eCA in CO_2 recovery as HCO_3^- and surface pH regulation were investigated, but eCA was found to have minimal effects on these processes.

To overcome the inefficiencies of Rubisco, many phytoplankton operate a CO_2-concentrating mechanism (CCM) that increases Rubisco's rate of carbon fixation and reduces oxygen fixation by increasing the concentration of CO_2 around the enzyme. CCMs typically consist of inorganic carbon (C_i) pumps, carbonic anhydrases (CAs) to equilibrate HCO_3^- and CO_2, and a compartment to confine Rubisco, such as the pyrenoid or carboxysome, minimizing the volume in which CO_2 is elevated (Badger et al., 1998; Kaplan and Reinhold, 1999; Giordano et al., 2005). Intracellular carbonic anhydrases (iCAs) play multiple roles in CCMs, including the conversion of accumulated HCO_3^- to CO_2 around Rubisco and the prevention of CO_2 leakage (Badger, 2003). Some organisms also have an extracellular carbonic anhydrase (eCA) associated with the cell wall, plasma membrane, or periplasmic space. The role of eCA has been enigmatic, although it is clearly related to the CCM. In *Chlamydomonas reinhardtii*, where eCA has been most thoroughly studied, the major eCA (Cah1) is up-regulated at low CO_2, and its regulatory network includes a transcription factor that induces the expression of other CCM genes as well (Yoshioka et al., 2004; Ohnishi et al., 2010). In other organisms, eCA activity generally increases, in some cases dramatically, at low CO_2, supporting its association with the CCM, but the genetic details of regulation are not known (Nimer et al., 1997; Rost et al., 2003).

When first discovered in microalgae, eCA was thought to facilitate CO_2 influx by keeping surface CO_2 at bulk solution concentrations (Moroney et al., 1985). Many microalgae take up CO_2 to support photosynthesis, but because of the low concentration of CO_2 in most natural waters and the slow rate of HCO_3^- dehydration, this uptake can lead to some depletion of CO_2 in the diffusive boundary layer surrounding the cell. eCA accelerates the dehydration of HCO_3^- to CO_2 within the boundary layer, increasing the surface CO_2 concentration. Support for this role has come from experiments showing that inhibition of eCA reduces photosynthetic rates and C_i accumulation in disparate microalgae, including the green alga *C. reinhardtii*, the dinoflagellate *Prorocentrum micans*, the prymnesiophyte *Phaeocystis globosa*, and the diatom *Thalassiosira weissflogii* (Moroney et al., 1985; Nimer et al., 1999; Elzenga et al., 2000; Burkhardt et al., 2001).

Although there is strong support for the role of eCA in CO_2 supply, some observations suggest that it may have additional or alternative roles. In some organisms,

[1] This work was supported by the National Science Foundation (grant nos. NSF EF 1041023 and MCB 1129326).

* Corresponding author; e-mail bmhopkin@uga.edu.

The author responsible for distribution of materials integral to the findings presented in this article in accordance with the policy described in the Instructions for Authors (www.plantphysiol.org) is: Brian M. Hopkinson (bmhopkin@uga.edu).

[W] The online version of this article contains Web-only data.

[OA] Open Access articles can be viewed online without a subscription.

www.plantphysiol.org/cgi/doi/10.1104/pp.113.217737

blocking eCA does not inhibit photosynthesis, and in *C. reinhardtii*, knocking out the major eCA had only minor effects on photosynthesis (Van and Spalding, 1999; Moroney et al., 2011). In *C. reinhardtii*, these results may be explained by the fact that only a small fraction of the total eCA activity is apparently required to support photosynthetic CO_2 uptake, so that if inhibition is not fully effective, CO_2 could still be kept high at the cell surface (Moroney et al., 1985; Palmqvist et al., 1990; Moroney et al., 2011). Such excess may point to other roles for eCA. On the basis of a correlation between HCO_3^- uptake and eCA activity, Trimborn et al. (2009) suggested that eCA in diatoms may be used to recover leaked CO_2, converting it to HCO_3^- to enhance uptake. eCA may also have a role in pH homeostasis, which is a common role for CA in heterotrophic organisms (Boron, 2004; Swietach et al., 2010).

We sought to better understand the role of eCA in two diatoms by making quantitative measurements of eCA rates and modeling the effect of eCA on boundary-layer chemistry. Our approach to quantify eCA activity is an adaptation of a common method to measure CA activity based on the enzyme's acceleration of ^{18}O removal from labeled C_i. This technique has been used to measure the kinetics of isolated CA enzymes (Silverman, 1982), iCA activity (Tu et al., 1978), and eCA activity (Palmqvist et al., 1994; Delacruz et al., 2010). The advance presented here is to extract a quantitative, intrinsic measure of surface eCA activity by applying a simple box model of ^{18}O-exchange kinetics to the data that accounts for the localization of the enzyme. In contrast, previous methods to measure eCA activity have effectively treated the activity as dispersed throughout the solution and, in some cases, are semiquantitative (Palmqvist et al., 1994; Elzenga et al., 2000; Delacruz et al., 2010). Previous approaches based on ^{18}O exchange use the long-term rate of ^{18}O removal as a quantitative but empirical measure of eCA activity (Palmqvist et al., 1994; Delacruz et al., 2010). Another technique uses the rate of equilibration of ^{14}C between CO_2 and HCO_3^-, quantifying eCA activity as an increase in the rate of CO_2 hydration in the bulk solution (Elzenga et al., 2000; Martin and Tortell, 2006). A key advantage of our approach is that eCA catalysis is treated as a surface phenomenon, allowing the measured activities to be used in modeling the effects of eCA on boundary-layer chemistry. Using the eCA rates measured in the diatoms, we assessed the potential role of eCA in CO_2 supply, CO_2 recovery, and pH homeostasis.

RESULTS

To determine eCA activity on the cell surface, paired measurements of ^{18}O-labeled C_i exchange were made in the presence and absence of an eCA inhibitor. When an eCA inhibitor is present, the ^{18}O-CO_2 data were used to determine iCA activity and CO_2 and HCO_3^- fluxes into the cell (Tu et al., 1978). Subsequently, surface eCA activity was quantified by comparing simulations using a model that describes the temporal evolution of the isotopologs of C_i in and around a cell (Fig. 1; see "Materials and Methods"), with ^{18}O removal rates measured in the absence of an eCA inhibitor.

iCA Kinetics and Mass Transfer Coefficients

Our method for the determination of eCA activity requires that iCA activity and mass transfer coefficients for passive CO_2 and HCO_3^- fluxes be known. These terms were determined from ^{18}O-removal kinetics when eCA activity was inhibited using the CA inhibitor acetazolamide (AZ) or dextran-bound acetazolamide (DBAZ; Tu et al., 1978; Hopkinson et al., 2011). iCA activities depended on culture conditions, ranging between 80 and 200 s^{-1} for *Thalassiosira pseudonana* and between 20 and 150 s^{-1} for *T. weissflogii*. Mass transfer coefficients for CO_2 (f_c) were $1.3 \pm 0.4 \times 10^{-8}$ cm^3 s^{-1} for *T. pseudonana* and $2.9 \pm 0.9 \times 10^{-8}$ cm^3 s^{-1} for *T. weissflogii*, while HCO_3^- mass transfer coefficients were less than 1×10^{-12} cm^3 s^{-1} for *T. pseudonana* and $1.9 \pm 1.6 \times 10^{-10}$ cm^3 s^{-1} for *T. weissflogii*, similar to previously reported values (Hopkinson et al., 2011).

Accurate determination of iCA activity and CO_2 and HCO_3^- mass transfer coefficients requires that eCA be fully inhibited. ^{18}O removal follows a biphasic pattern in which there is an initial, rapid removal of ^{18}O as CO_2 enters CA-containing cells followed by a slower, long-term loss of ^{18}O due to the depletion of ^{18}O from HCO_3^- (Silverman et al., 1976; Fig. 2). We used the long-term rate of ^{18}O removal or "phase II slope" (calculated as the slope of a linear fit through natural log-transformed ^{18}O atom fraction data) as an empirical measure of eCA activity to establish that eCA effectively inhibited the CA inhibitors (Fig. 3; Delacruz et al., 2010). Application of increasing concentrations of AZ or DBAZ to cells expressing eCA reduces the phase II slope to near background, uncatalyzed exchange rates, verifying that eCA activity was effectively eliminated. The presence of iCA accelerates long-term ^{18}O removal slightly above

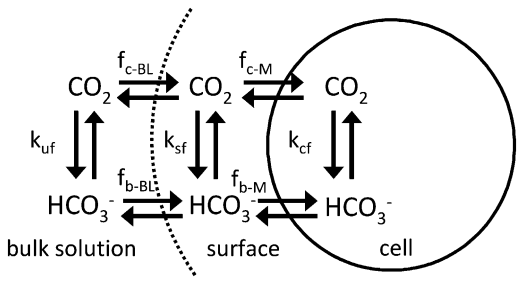

Figure 1. Diagram of the compartments and fluxes in the box model used to determine eCA activity (Eqs. 1–6; Table III). Fluxes between the compartments are described using mass transfer coefficients, and the reactions are treated using first-order rate constants.

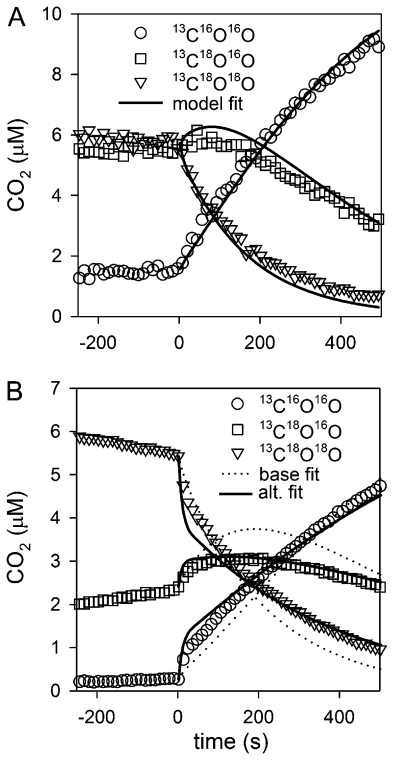

Figure 2. Sample model fits to ^{18}O-CO_2 data for the determination of eCA activity. Cells expressing eCA were added to the assay solution at time 0, accelerating ^{18}O removal. A shows a good fit to the data. B shows an example where a better fit can be achieved by reducing $f_{b\text{-}BL}$ 10-fold, but the eCA activities are similar in both fits (base, $k_{sf} = 1.7 \times 10^{-6}$; reduced, $f_{b\text{-}BL}\ k_{sf} = 1.5 \times 10^{-6}$). For clarity, only every other ^{18}O-CO_2 data point is shown.

the background rate. We verified that neither AZ nor DBAZ had a detectable effect on iCA activity of low-pH-grown cells (where eCA is absent; see below) and so did not pass through the plasma membrane to any significant extent (data not shown).

Determination of eCA Rate Constants

After determining the rate constants for iCA and CO_2 and HCO_3^- mass transfer coefficients, eCA activity in *T. pseudonana* and *T. weissflogii* was quantified by fitting the box model of isotope exchange to the observations (see Eqs. 1–6 in "Materials and Methods"). k_{sf}, the first-order rate constant for eCA-catalyzed CO_2 hydration, is used as a measure for eCA activity, since it can be directly compared with the boundary-layer mass transfer coefficient for CO_2 ($f_{c\text{-}BL}$) to assess the effectiveness of eCA (see "Materials and Methods"). The model gave good fits to the ^{18}O-CO_2 data in most cases, and the eCA activities were consistent in replicate runs (Fig. 2A). eCA activities (k_{sf}) varied with culture and assay conditions, ranging between 0 and 3.5×10^{-7} $cm^3\ s^{-1}$ for *T. pseudonana* and between 0 and 40×10^{-7} $cm^3\ s^{-1}$ for *T. weissflogii*.

In some runs, the model fits could not account for a depletion of the $^{13}C^{18}O^{16}O$ intermediate species later in the assay (Fig. 2B). This signature suggests reduced exchange between the surface layer and the bulk solution (Silverman et al., 1981), and the fit can be improved by reducing the diffusive HCO_3^- flux to the cell surface (e.g. due to the presence of an extracellular matrix that reduces the diffusivity of charged ions; Stewart, 2003). However, this improvement of the fit alters the estimated eCA activity by less than 20% (Fig. 2B). Similarly, eCA activity is not sensitive to the choice of the size of the surface boundary-layer volume (Table I). The effect of potential residual eCA activity when determining iCA rate constants and cross-membrane fluxes was also assessed using the eCA box model. eCA activity and HCO_3^- permeability have similar effects on ^{18}O-CO_2 behavior, because both expose the extracellular HCO_3^- pool to CA and so accelerate the long-term rate of ^{18}O removal. If eCA was not fully inhibited during the determination of iCA activity and mass transfer coefficients, the activity would be treated as increased HCO_3^- transfer through the cell membrane (greater $f_{b\text{-}M}$). To determine the maximal residual eCA activity, we fit ^{18}O-CO_2 data from runs in which eCA should have been completely inhibited (50 μM or greater AZ or DBAZ) to the eCA box model (Eqs. 1–6), setting HCO_3^- membrane permeability to zero ($f_{b\text{-}M} = 0$) and treating iCA activity (k_{cf}), CO_2 permeability ($f_{c\text{-}M}$), and eCA activity (k_{sf}) as unknowns. The potential residual eCA activities (*T. pseudonana*, $5.2 \pm 7.1 \times 10^{-9}$ $cm^3\ s^{-1}$; *T. weissflogii*, $5.4 \pm 4.6 \times 10^{-8}$ $cm^3\ s^{-1}$) were low relative to measured eCA activities. Thus, both the empirical analysis (Fig. 3) and the modeling approach show that the eCA inhibitors were highly effective.

eCA Kinetics: Effect of pH and C_i

To characterize eCA enzyme kinetics, strong eCA activity was induced by growing cultures to high density

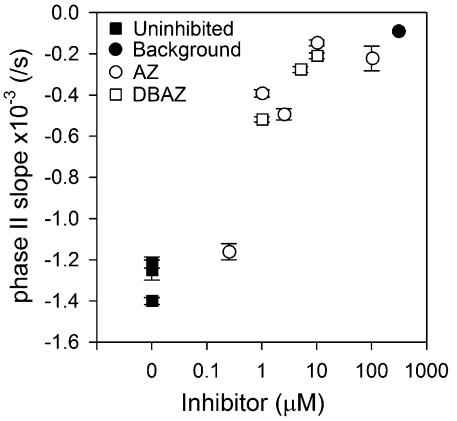

Figure 3. Long-term rate of ^{18}O removal (phase II slope) as a function of eCA inhibitor concentration. The background rate, prior to cell addition, is also plotted.

Table I. *Effect of model surface volume on derived eCA activity*

Surface Volume	eCA Activity
cm^3	$cm^3\ s^{-1}$
2.0×10^{-12}	7.29×10^{-8}
8.2×10^{-12}	7.34×10^{-8}
4.8×10^{-11}	7.31×10^{-8}
1.1×10^{-10}	7.32×10^{-8}

without pH or CO_2 control (final culture pH of 8.6–8.8). The cells were then concentrated and immediately assayed for eCA activity at a range of pHs and C_i concentrations. Enzyme activity (k_{sf}) increased linearly with pH in *T. pseudonana* (7.8–8.6) and in *T. weissflogii* (7.5–8.4; Fig. 4, A and B) over a pH range typical of marine environments. CA activity typically shows a logarithmic increase with pH as water at the active site is deprotonated (Silverman and Lindskog, 1988). Our observations indicate a linear response, which may reflect the small pH range tested or result from differences between solution and cell surface pH.

We assessed the effect of C_i concentration on eCA reaction rates. eCA activity was measured at pH 7.9 and varying C_i from 0.5 to 12 mM, with corresponding CO_2 concentrations ranging from 5 to 115 μM (Fig. 4, C and D). In *T. pseudonana*, nonlinearity in the reaction rate (CO_2 hydration rate) versus substrate concentration (CO_2) was observed only at the very highest CO_2 concentration. In *T. weissflogii*, there is more significant nonlinearity, allowing a Michaelis-Menten function to be fit to the data. From this fit, the half-saturation constant of eCA for CO_2 is 87 ± 10 μM. These results show that CO_2 hydration and HCO_3^- dehydration are effectively first order with respect to substrate concentration in the environmentally relevant range (approximately 2 mM C_i, CO_2 of 5–20 μM), validating our use of a first-order rate constant as a measure of eCA activity.

eCA Expression: Effect of CO_2 and pH

T. pseudonana and *T. weissflogii* were grown for several generations at different pHs (7.7–8.6) maintained by a pH buffer 4-(2-Hydroxyethyl)piperazine-1-propanesulfonic acid (EPPS) at constant C_i (2 mM), concentrated, and assayed for eCA activity at constant pH (8.0) and C_i (2 mM) to determine the effect of growth conditions on eCA expression. Under these culture conditions, pH and CO_2 covary with CO_2, ranging between 24 μM at pH 7.8 and 3 μM at pH 8.6. In *T. pseudonana*, eCA activity was undetectable from pH 7.8 to 8.1 but then increased dramatically above this pH (Fig. 5A). eCA activity in *T. weissflogii* was undetectable only in cells grown at the lowest pH (7.8) and then increased quickly to a high, constant value from pH 8.0 to 8.6 (Fig. 5B). iCA activity (k_{cf}) also increased substantially from low to high culture pH in both species (*T. pseudonana*, 80–200 s^{-1}; *T. weissflogii*,

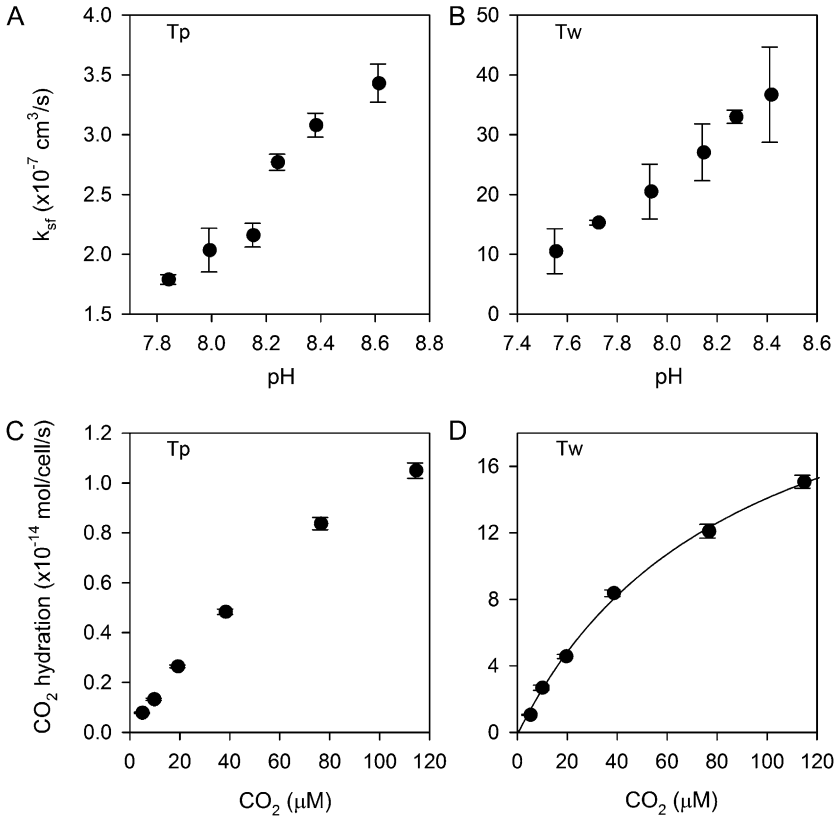

Figure 4. eCA kinetics. A and B, Effects of assay pH on eCA activity in *T. pseudonana* (Tp; A) and *T. weissflogii* (Tw; B). C and D, Reaction rates (CO_2 hydration rate) as a function of substrate concentration (CO_2) in *T. pseudonana* (C) and *T. weissflogii* (D). A Michaelis-Menten fit to the *T. weissflogii* data, which shows some saturation, gives a CO_2 half-saturation constant of 87 ± 10 μM and a maximal reaction rate of 26 ± 2 × 10^{-14} mol cell^{-1} s^{-1}.

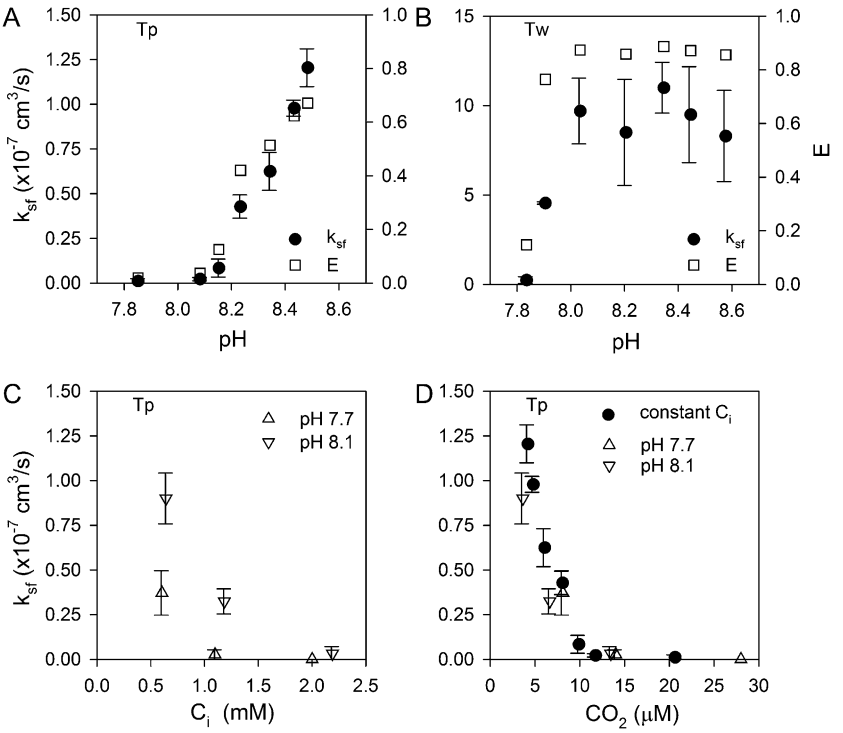

Figure 5. Expression of eCA as a function of culture pH and C_i. A and B, When grown at a constant total C_i (2 mM) but varying pH, both diatoms induce eCA at high pH/low CO_2 (A, *T. pseudonana* [Tp]; B, *T. weissflogii* [Tw]). The level of activity is sufficient to reduce surface-to-bulk CO_2 gradients, as shown by the effectiveness index (E; Eq. 13). C, When *T. pseudonana* was grown at constant pH (7.7 or 8.1) but varying C_i, eCA was induced at low C_i. D, All the *T. pseudonana* data converge when plotted as a function of CO_2, showing that it is the major control on eCA expression.

20–150 s^{-1}). Complementary experiments in which the culture pH was held constant but C_i was varied also showed that low CO_2 induced eCA expression in *T. pseudonana* (Fig. 5C). The *T. pseudonana* eCA activity data from the constant C_i and constant pH experiments converge, following a single trend, when plotted as a function of CO_2 concentration in the growth medium, showing that eCA expression was primarily controlled by CO_2 (Fig. 5D).

Effect of eCA Inhibition on Photosynthesis

We tested the effects of short-term eCA inhibition on photosynthesis. At a concentration of AZ sufficient to inhibit all detectable eCA activity (50 μM), there was no consistent effect of short-term eCA inhibition on photosynthesis under environmentally relevant conditions of C_i availability (C_i, 2 mM; pH 7.8–8.6; Fig. 6A). We assessed the effects of AZ ranging from 1 to 500 μM on photosynthesis in *T. pseudonana* and *T. weissflogii* grown without pH control to pH 8.7 and assayed at the same pH, but we found no significant inhibition of photosynthesis even at the highest AZ concentrations (data not shown). Only at very low CO_2 concentrations (1 μM; pH 8.7; C_i, 1 mM) did short-term eCA inhibition consistently reduce photosynthesis, inhibiting oxygen production by 42% ± 5% in *T. weissflogii* and by 25% ± 8% in *T. pseudonana* (Fig. 6B).

Effect of eCA Inhibition on Growth

To test the long-term effects of eCA inhibition, growth rates of the two diatoms were measured in the presence and absence of DBAZ (Table II). The cultures were grown for 4 to 6 d under the same environmental conditions as other cultures (20°C, 16/8-h photoperiod at 125–150 μmol photons m^{-2} s^{-1}) with 20 μM DBAZ added initially and 5 μM additional DBAZ added in the morning of day 3. In *T. weissflogii*, DBAZ reduced growth by approximately 10% at pH 8.4 (5 μM CO_2) but had no effect on growth at pH 7.8 (24 μM CO_2), demonstrating that the inhibitor did not have any nonspecific effects on metabolism. DBAZ had no significant effect on growth of *T. pseudonana* at pH 8.4.

Model Assessment of eCA on Surface Boundary-Layer Chemistry

We used a spatially resolved reaction-diffusion model of the diffusive boundary layer to quantify the effect of eCA on boundary-layer chemistry (for details, see "Materials and Methods"). The primary role of eCA is thought to be the maintenance of bulk solution CO_2 concentrations at the cell surface during photosynthesis. To assess this role, a model simulation was run in which a diatom takes up CO_2 at two-thirds its photosynthetic rate, which is typical of cultured marine diatoms (Burkhardt et al., 2001; Rost et al., 2003; Hopkinson et al., 2011). Average photosynthetic rates measured in this study were used in the simulation (*T. pseudonana*, 1.7×10^{-17} mol $cell^{-1}$ s^{-1}; *T. weissflogii*, 7×10^{-17} mol $cell^{-1}$ s^{-1}). The analysis shows that the measured eCA activities are sufficient to maintain cell surface CO_2 near bulk concentrations despite photosynthetic carbon uptake in both species (Fig. 7). In all cases, however, the absolute size of the CO_2 gradient is

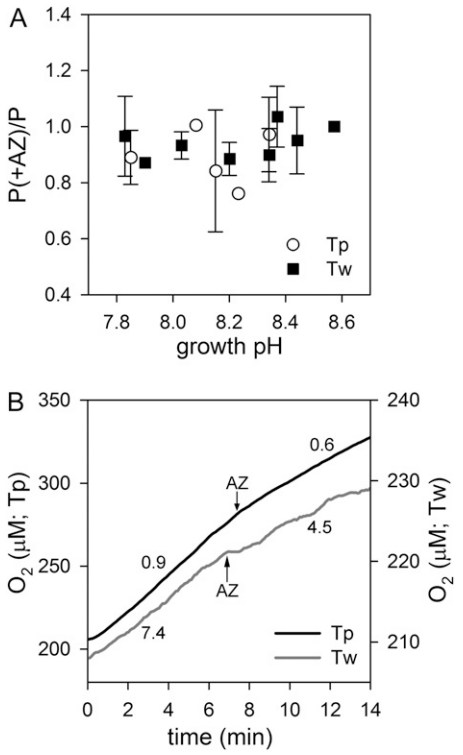

Figure 6. Effect of the eCA inhibitor AZ on photosynthesis. A, Effect of short-term inhibition of eCA on photosynthesis shown as the ratio of the photosynthetic rate in the presence of the inhibitor (P+AZ) to the rate without the inhibitor (P). The diatoms (*T. pseudonana* [Tp] and *T. weissflogii* [Tw]) were grown and assayed at a range of pHs with constant C_i (2 mM). B, Oxygen traces showing inhibition of photosynthesis at 1 μM CO_2 after the addition of AZ. The numbers next to the traces indicate the rate of oxygen production ($\times 10^{-17}$ mol cell^{-1} s^{-1}) before and after AZ addition.

relatively small. In the absence of eCA, the concentration difference between the bulk solution and the cell surface is only 0.2 μM for *T. pseudonana* and 0.35 μM for *T. weissflogii*.

An alternative role for eCA in the recovery of leaked CO_2 as HCO_3^- for subsequent uptake has also been suggested (Trimborn et al., 2008). As CO_2 leakage is just the inverse of CO_2 uptake, the modeled effects of eCA on CO_2 gradients are very similar. In both diatoms, fully induced eCA activity is able to convert nearly all the leaked CO_2 to HCO_3^-. However, even when eCA is effective, the changes in surface HCO_3^- concentrations are minuscule. The largest increase in HCO_3^- concentration is 0.7 μM, which is only a 0.04% increase (Fig. 8A).

Finally, eCA could also be involved in the control of surface pH, since the C_i system dominates pH buffering in seawater. One scenario, discussed below, involves H^+ uptake equimolar to HCO_3^- uptake to compensate for intracellular H^+ consumption required to convert HCO_3^- to CO_2 for photosynthesis. This scenario was simulated with rates of H^+ and HCO_3^- uptake at the cell surface equal to photosynthetic rates, but we found that eCA activity had no effect on the surface H^+ perturbation induced by this uptake, because of rapid acid/base equilibration among buffer species (data not shown). CO_2 uptake creates a pH disequilibrium in the boundary layer that can be reestablished by eCA (Fig. 8B), but the effect on the H^+ concentration is very small.

DISCUSSION

Although there is strong evidence that eCA is linked to the CCM, its exact role has been controversial (Van and Spalding, 1999; Trimborn et al., 2008; Moroney et al., 2011). Enhancement of CO_2 availability for photosynthesis is the most logical role for eCA, since CO_2 concentrations are low in most natural waters and can become depleted in cell boundary layers. But alternative roles in the recovery of leaked CO_2 and pH homeostasis have also been suggested, based in part on observations that the elimination of eCA does not always reduce photosynthesis. The lack of a quantitative, intrinsic measure of eCA activity has hindered the evaluation of its role. Here, we have developed an approach to quantify eCA activity, applied it to two marine diatoms, and evaluated the potential role of eCA in these organisms through an analysis of the effect of eCA activity on surface boundary-layer chemistry.

Enhancement of CO_2 Supply

eCA is commonly thought to facilitate CO_2 influx by dehydrating HCO_3^- at the cell surface. Many microalgae take up CO_2 for photosynthesis (Badger et al., 1994; Burkhardt et al., 2001), which is most likely driven by a diffusive gradient (Kaplan and Reinhold, 1999; Hopkinson et al., 2011), despite the fact that HCO_3^- is much more abundant than CO_2 in the ocean. Net CO_2 uptake into the cell can be supported either by diffusion of CO_2 from the bulk solution or generation of CO_2 from HCO_3^- within the boundary layer, which for microalgae would need to be catalyzed by eCA because uncatalyzed HCO_3^- dehydration is slow (Wolf-Gladrow and Riebesell, 1997).

Consistent with a role for eCA in CO_2 supply, we find that eCA is up-regulated at low CO_2 concentrations and that induction occurs at a higher CO_2 concentration in the larger diatom *T. weissflogii*, which is more prone to diffusive limitation (Fig. 5; Pasciak and

Table II. *Effect of DBAZ on growth rate*

The asterisk indicates that the DBAZ treatment was significantly different ($P < 0.05$; $n = 4$) from the control based on Student's *t* test.

Diatom	Culture pH	Growth Rate	
		Control	DBAZ
		$d^{-1} \pm SD$	
T. pseudonana	8.4	1.15 ± 0.01	1.14 ± 0.02
T. weissflogii	8.4	0.55 ± 0.01	0.51 ± 0.03*
T. weissflogii	7.8	0.94 ± 0.02	0.94 ± 0.02

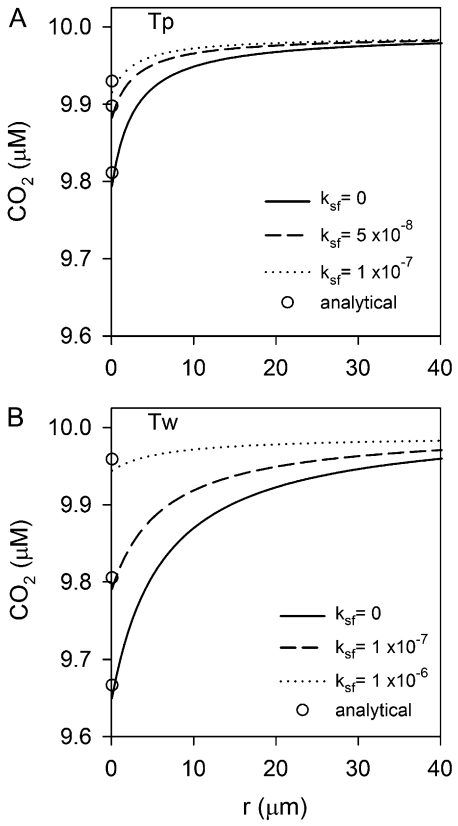

Figure 7. Model simulations of the effect of eCA on surface boundary-layer chemistry during CO_2 uptake. (A, *T. pseudonana* [Tp]; B, *T. weissflogii* [Tw]). The effect of eCA on the CO_2 profiles is shown at two eCA activities, the lower at a magnitude similar to $f_{c\text{-}BL}$ and the higher approximating maximal expression levels. k_{sf} values used in the simulations are indicated. Analytical approximations for surface CO_2 concentrations obtained using Equation 12 are indicated with white circles, agreeing well with the numerical solution.

Gavis, 1974; Riebesell et al., 1993). Typically, the effect of CO_2 on eCA expression is assessed by varying pH at a constant C_i concentration or by bubbling cultures with air containing varying levels of CO_2 (Nimer et al., 1997; Rost et al., 2003). In both approaches, CO_2 and pH are closely coupled, with CO_2 decreasing as pH increases, but it is generally assumed that CO_2 is the key variable regulating eCA activity. Both *T. pseudonana* and *T. weissflogii* expressed eCA at low CO_2/high pH (Fig. 5, A and B) in such an experiment, as is commonly observed. But by additionally culturing *T. pseudonana* at constant pH but variable C_i (Fig. 5C), we were able to clearly show that eCA activity responds to low CO_2 concentrations, rather than changes pH or HCO_3^-, consistent with a role for eCA in CO_2 uptake (Fig. 5D).

A key finding, made possible by the quantitative nature of the eCA measurements, is that the amount of eCA expressed by both diatoms is appropriate to support CO_2 uptake, but not excessive. As shown in Equations 11 to 13 (see "Materials and Methods"), the relative magnitude of the boundary-layer mass transfer coefficient ($f_{c\text{-}BL}$) and eCA activity (k_{sf}) controls the sources of CO_2 (diffusion or dehydration) for net uptake and describes the extent to which eCA is able to mitigate CO_2 drawdown in the boundary layer. eCA activity at low CO_2 in *T. pseudonana* and *T. weissflogii* is two to 10 times greater than the boundary-layer mass transfer coefficient ($f_{c\text{-}BL}$; *T. pseudonana*, 5.9×10^{-8} cm^3 s^{-1}; *T. weissflogii*, 1.4×10^{-7} cm^3 s^{-1}), such that eCA activity is nearly optimal for the abolishment of bulk solution to surface CO_2 gradients (Fig. 5). A spatially resolved model confirms that the eCA activities are able to maintain surface CO_2 concentrations at near bulk concentrations (Fig. 7; for model description, see "Materials and Methods"). The lack of excess eCA for CO_2 supply in these diatoms contrasts with *C. reinhardtii*, where there is apparently excess eCA for CO_2 supply (Moroney et al., 1985), which could be taken to imply that it has other roles.

While the magnitude of the CO_2 drawdown at the cell surface is relatively small (0.2–0.35 μM; Fig. 7), it is similar in size to the CO_2 gradient across the cytoplasmic membrane that drives CO_2 influx. For example,

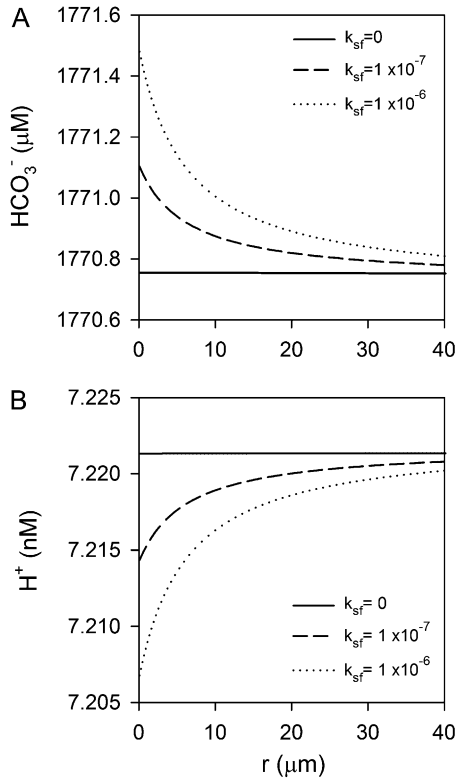

Figure 8. Model simulations showing that the effects of eCA on surface boundary-layer HCO_3^- and H^+ concentrations are small. A, If CO_2 leaks from the cell, eCA can convert this leaked CO_2 to HCO_3^-, but the surface HCO_3^- concentration increases by less than 1 μM. B, eCA has only a minor effect on the H^+ concentration during CO_2 uptake. Both panels show results from simulations with *T. weissflogii*, since the effects of eCA, although still small, are more significant for this species.

given the permeability of the *T. weissflogii* membrane to CO_2 (Hopkinson et al., 2011), a 0.4 μM CO_2 gradient across the plasma membrane would be needed to support CO_2 uptake at the rate estimated for our culture conditions. The high permeability of membranes to CO_2 means that this influx occurs passively, which is potentially more energy efficient than active uptake of HCO_3^-, but requires the cell to generate a CO_2 gradient across the cytoplasmic membrane. In the absence of eCA, intracellular CO_2 would need to be drawn down further to maintain CO_2 uptake, which diatoms are capable of doing, as shown by their ability to take up CO_2 over a wide range of extracellular CO_2 concentrations (Burkhardt et al., 2001), but at the cost of increased energetic expenditure.

Short-term inhibition of eCA at CO_2 concentrations greater than 1 μM did not reduce photosynthesis, presumably because cytoplasmic CO_2 concentrations could be lowered to maintain CO_2 influx (Fig. 6A). Photosynthesis was only reduced when extracellular CO_2 concentrations decreased to 1 μM (Fig. 6B), at which point the cytoplasmic CO_2 concentration was 0.4 μM in *T. pseudonana* and 0.2 μM in *T. weissflogii*, as estimated using boundary-layer mass transfer coefficients and the cytoplasmic membrane permeability for each species. The cells apparently could not lower their intracellular CO_2 concentrations further, and for *T. weissflogii*, the intracellular CO_2 concentration was so low that greater reduction would not significantly increase CO_2 influx. Long-term inhibition of eCA reduced the growth of *T. weissflogii* at low CO_2 (Table II), consistent with an increased energetic cost of C_i acquisition without eCA, although inhibition of eCA had no detectable effect on the growth of *T. pseudonana*, perhaps because its smaller size minimizes the magnitude of the bulk-to-surface CO_2 gradient and the energetic costs associated with compensating for this gradient. However, even a small energetic savings that allows minor increases in growth rate can have major consequences for the ecological success of plankton in the ocean (Tilman, 1977).

Alternative Roles for eCA

Alternative roles for eCA in the recovery of leaked CO_2 and the regulation of cell surface pH have been suggested (Trimborn et al., 2008). The CCM is not perfectly efficient, in large part because of the high permeability of membranes to CO_2, leading to CO_2 leakage out of the chloroplast or plasma membranes. While eCA could effectively convert leaked CO_2 to HCO_3^-, the increase in HCO_3^- concentration achieved by CO_2 recovery would be very small compared with the approximately 1.8 mM HCO_3^- concentration in seawater (Fig. 8A). Assuming that diatom HCO_3^- transporters follow Michaelis-Menten kinetics, in which the greatest sensitivity of uptake rate to substrate is a linear increase at low substrate concentrations, the increased cell surface HCO_3^- concentration would allow at most a 0.04% increase in uptake rate. Additionally, diatoms exhibit a net CO_2 influx rather than a net CO_2 efflux under normal conditions (Burkhardt et al., 2001; Hopkinson et al., 2011), so there is no CO_2 leaking from the cell to be recovered.

CAs are commonly involved in pH regulation (Boron, 2004), so it is conceivable that eCA may be involved in pH maintenance, since the C_i system is the main pH buffer in seawater. The best example of the role

Table III. *Model notation*

Boldface symbols denote concentration vectors: $\mathbf{c}$ = [$C^{16}O_2$; $C^{16}O^{18}O$; $C^{18}O_2$]; $\mathbf{b}$ = [$HC^{16}O_3^-$; $HC^{16}O_2{}^{18}O^-$; $HC^{16}O^{18}O_2^-$; $HC^{18}O_3^-$].

Symbol	Definition	Units	Source/Method Reference
$\mathbf{c_e}$	Concentration of ^{18}O-CO_2 species in the bulk solution	mol cm^{-3}	MIMS measurement
$\mathbf{c_s}$	Concentration of ^{18}O-CO_2 species in the surface boundary layer	mol cm^{-3}	Modeled
$\mathbf{c_i}$	Concentration of ^{18}O-CO_2 species inside the cell	mol cm^{-3}	Modeled
$\mathbf{b_e}$	Concentration of ^{18}O-HCO_3^- species in the bulk solution	mol cm^{-3}	Modeled
$\mathbf{b_s}$	Concentration of ^{18}O-HCO_3^- species in the surface boundary layer	mol cm^{-3}	Modeled
$\mathbf{b_i}$	Concentration of ^{18}O-HCO_3^- species inside the cell	mol cm^{-3}	Modeled
k_{uf}	Uncatalyzed CO_2 hydration rate constant	s^{-1}	Background ^{18}O removal rate
k_{ur}	Uncatalyzed HCO_3^- dehydration rate constant	s^{-1}	Background ^{18}O removal rate
k_{sf}	eCA-catalyzed CO_2 hydration rate constant	cm^3 s^{-1}	eCA assay (this study)
k_{sr}	eCA-catalyzed HCO_3^- dehydration rate constant	cm^3 s^{-1}	eCA assay (this study)
k_{cf}	iCA-catalyzed CO_2 hydration rate constant	s^{-1}	iCA assay (Tu et al., 1978)
k_{cr}	iCA-catalyzed HCO_3^- dehydration rate constant	s^{-1}	iCA assay (Tu et al., 1978)
$f_{c\text{-}BL}$	Boundary-layer mass transfer coefficient for CO_2	cm^3 s^{-1}	iCA assay (Tu et al., 1978)
$f_{b\text{-}BL}$	Boundary-layer mass transfer coefficient for HCO_3^-	cm^3 s^{-1}	iCA assay (Tu et al., 1978)
$f_{c\text{-}M}$	Membrane mass transfer coefficient for CO_2	cm^3 s^{-1}	iCA assay (Hopkinson et al., 2011)
$f_{b\text{-}M}$	Membrane mass transfer coefficient for HCO_3^-	cm^3 s^{-1}	iCA assay (Hopkinson et al., 2011)
N	Number of cells in the assay chamber	–	Coulter Counter measurement
V_e	Bulk solution volume	cm^3	Measured
V_s	Surface layer volume	cm^3	Imposed, 8×10^{-12} cm^3
V_i	Intracellular volume	cm^3	Coulter Counter measurement
G	Stoichiometric matrix describing the hydration of CO_2 species to HCO_3^-	–	Hopkinson et al. (2011)
H	Stoichiometric matrix describing the dehydration of HCO_3^- species to CO_2	–	Hopkinson et al. (2011)

of eCA in pH maintenance comes from human cancer cells, where high rates of respiration lead to a high acid load (in the form of CO_2). By converting CO_2 to HCO_3^- and H^+ outside the cell, eCA helps to maintain an alkaline internal environment at the expense of a more acidic extracellular environment (Swietach et al., 2010). Photosynthetic organisms such as diatoms, on the other hand, import CO_2 and HCO_3^- for carbon fixation. Since CO_2 is ultimately the species fixed by Rubisco, the import and subsequent consumption of CO_2 has no net effect on intracellular acid/base balance. However, imported HCO_3^- must be converted to CO_2 for fixation, consuming a proton in the process. Organisms that transport HCO_3^- then need to import a proton (or export OH^-) for each molecule of HCO_3^-. eCA could help supply H^+ to the cell surface to balance HCO_3^- uptake, potentially accounting for the observed correlation between eCA and HCO_3^- uptake in several marine phytoplankton (Trimborn et al., 2008). Simulation of the effect of eCA on boundary-layer pH for diatoms importing HCO_3^- and H^+ revealed that the boundary-layer pH changes induced by uptake are very small because of rapid reactions among the buffer species HCO_3^-/CO_3^{2-} and $B(OH)_4^-/B(OH)_3$. Furthermore, eCA does not alter the small pH changes, because the slow CO_2/HCO_3^- equilibrium is not significantly involved in boundary-layer pH buffering in this case. Alternatively, eCA could help establish pH equilibrium during CO_2 uptake. We simulated the effect of eCA on boundary-layer pH, assuming that the diatoms obtain all their carbon for photosynthesis from CO_2. eCA does have an effect on boundary-layer pH in this case, and the highest rates are effective at reestablishing pH equilibrium, but the absolute effect of eCA on H^+ concentration is very small (Fig. 8B).

CONCLUSION

Using a newly developed approach to quantify eCA-catalyzed CO_2 hydration rates, eCA activity was measured in two diatoms, *T. pseudonana* and *T. weissflogii*, and its potential roles in CO_2 supply, CO_2 recovery, and pH regulation were investigated. In support of the role of eCA in photosynthetic CO_2 supply, its activity increased at low CO_2 concentrations, was appropriate to abolish bulk-to-surface CO_2 gradients, and was greater in the larger diatom (*T. weissflogii*), which is more prone to diffusive limitation. The differences in CO_2 concentration between the bulk solution and the cell surface that are eliminated by eCA are small (less than 0.5 μM), but small gradients drive significant passive CO_2 influxes in these diatoms (Hopkinson et al., 2011). The consequences of short-term inhibition of eCA can be overcome by decreasing the cytoplasmic CO_2 concentration to maintain CO_2 influx rates. However, this requires increased energetic expenditure, which may explain the decreased growth rate of *T. weissflogii* when eCA was inhibited. We investigated alternative roles for eCA in the recovery of leaked CO_2 for HCO_3^- uptake and pH regulation but found that eCA activity would not have a significant effect on boundary-layer HCO_3^- and H^+ concentrations. Taken together, these results support a role for eCA in CO_2 supply.

MATERIALS AND METHODS

Culturing

The diatoms *Thalassiosira pseudonana* (CCMP1335) and *Thalassiosira weissflogii* (CCMP1336) were obtained from the National Center for Marine Algae and Microbiota and maintained in Aquil medium (Price et al., 1988). For most experimental work, the algae were grown in Aquil made from a natural seawater base with 5 mM 4-(2-Hydroxyethyl)piperazine-1-propanesulfonic acid (EPPS) buffer to maintain constant pH and C_i conditions. To assess the pH and C_i dependence of enzyme kinetics, cultures were grown in Aquil to high density without pH or CO_2 control (final culture pH of 8.6–8.8) to induce strong eCA activity. For experiments in which C_i concentrations were varied, North East Pacific Culture Collection Enriched Seawater, Artificial Seawater (NEPCC ESAW) medium was used with 5 mM EPPS buffer added (Harrison et al., 1980). This medium uses an artificial seawater base, and C_i was left out in the initial medium preparation, being added later at the desired concentration. All cultures were grown in an incubator at 20°C under fluorescent lights (125–150 μmol photons m^{-2} s^{-1}) on a light/dark cycle (16 h on, 8 h off). Cell numbers were counted daily with a Coulter Counter, and cells were harvested during exponential growth.

The initial pH of the culture medium was adjusted with HCl or NaOH (stored in sealed serum vials to avoid CO_2 absorption) and measured on the total hydrogen ion scale using thymol blue (Zhang and Byrne, 1996). The C_i concentration was measured at the beginning and end of the experiments using membrane inlet mass spectrometry (MIMS; Beckmann et al., 2009; Hopkinson et al., 2011). Additional carbon system parameters (CO_2, HCO_3^-, and CO_3^{2-} concentrations) were calculated from pH and C_i (Dickson and Goyet, 1994; Lueker et al., 2000).

^{18}O-Exchange Experiments

The rate of ^{18}O removal from labeled C_i was used to determine iCA and eCA activities. ^{18}O-labeled ^{13}C-C_i (2 mM, unless otherwise noted) was added to assay buffer (C_i-free artificial seawater, 20 mM Tris at pH 8.0, unless otherwise noted) in a MIMS chamber. Temperature in the chamber was maintained at 20°C using a water jacket. ^{18}O-CO_2 species were monitored by MIMS for approximately 10 min to determine the background rate of CO_2 hydration/HCO_3^- dehydration, after which cells were added to the chamber from a concentrated suspension. ^{18}O removal catalyzed by cellular CA was then monitored in the dark for 15 to 20 min. To determine iCA activity, an inhibitor of eCA was added prior to the addition of cells. In most cases, 50 μM AZ was used, but 50 μM DBAZ (Ramidus) was used in select experiments to confirm that diatom membranes were not permeable to AZ.

Photosynthetic Rates

The effect of eCA inhibitors on photosynthesis was assessed from measurements of oxygen production made using MIMS. Assay buffer with 2 mM C_i, unless otherwise noted, was added to the MIMS chamber, and cells were added from a concentrated suspension. Light was provided from a tungsten lamp at 200 μmol photons m^{-2} s^{-1}. Oxygen production was monitored for approximately 10 min, at which point AZ or DBAZ was added and oxygen production was monitored for a further approximately 10 min. Measurements were made at the same pH as the cultures were grown and at pH 8.0.

eCA Model Development

The eCA box model considers ^{18}O-CO_2 and ^{18}O-HCO_3^- isotopologs in three compartments: the bulk solution, the boundary layer at the cell surface, and the intracellular space (Fig. 1; Table III). Fluxes between the compartments are described by mass transfer coefficients, and the uncatalyzed and catalyzed CO_2 hydration/HCO_3^- dehydration reactions, responsible for ^{18}O removal,

are treated as first-order reactions, since the enzyme is undersaturated for C_i (Fig. 4). The model is described by the following system of differential equations:

$$\frac{d\mathbf{c_e}}{dt} = -k_{uf}\mathbf{c_e} + k_{ur}\mathbf{Hb_e} + \frac{f_{c-BL}N}{V_e}(\mathbf{c_s}-\mathbf{c_e}) \quad (1)$$

$$\frac{d\mathbf{b_e}}{dt} = k_{uf}\mathbf{Gc_e} - k_{ur}\mathbf{b_e} + \frac{f_{b-BL}N}{V_e}(\mathbf{b_s}-\mathbf{b_e}) \quad (2)$$

$$\frac{d\mathbf{c_s}}{dt} = \frac{N}{V_s}\left(-k_{sf}\mathbf{c_s} + k_{sr}\mathbf{Hb_s} + f_{c-BL}(\mathbf{c_e}-\mathbf{c_s}) + f_{c-M}(\mathbf{c_i}-\mathbf{c_s})\right) \quad (3)$$

$$\frac{d\mathbf{b_s}}{dt} = \frac{N}{V_s}\left(k_{sf}\mathbf{Gc_s} - k_{sr}\mathbf{b_s} + f_{b-BL}(\mathbf{b_e}-\mathbf{b_s}) + f_{b-M}(\mathbf{b_i}-\mathbf{b_s})\right) \quad (4)$$

$$\frac{d\mathbf{c_i}}{dt} = k_{cf}\mathbf{c_i} + k_{cr}\mathbf{Hb_i} + \frac{f_{c-M}N}{V_i}(\mathbf{c_s}-\mathbf{c_i}) \quad (5)$$

$$\frac{d\mathbf{b_i}}{dt} = k_{cf}\mathbf{Gc_i} - k_{cr}\mathbf{b_i} + \frac{f_{b-M}N}{V_i}(\mathbf{b_s}-\mathbf{b_i}) \quad (6)$$

with variables and parameters as described in Table III.

The solution volume (V_e) was measured directly, and the intracellular volume was determined using a Coulter Counter. The volume of the boundary layer compartment (V_s) was set to 8×10^{-12} cm^3, reflecting a surface layer thickness on the order of 0.1 μm. The uncatalyzed CO_2 hydration/HCO_3^- dehydration rates in the bulk solution (k_{uf}, k_{ur}) were determined from ^{18}O removal rates prior to the addition of cells, and the observed values agree well with published rates (Johnson, 1982). The mass transfer coefficients for diffusive flux between the bulk solution and the boundary layer ($f_{c\text{-}BL}$, $f_{b\text{-}BL}$) were calculated assuming the cells are spherical, with radii determined from Coulter Counter measurements (*T. pseudonana*, 2.5 μm; *T. weissflogii*, 6 μm):

$$f_{c-BL} = 4\pi RD, \quad (7)$$

where R is the cell radius and D is the diffusivity of CO_2 (1.65×10^{-5} cm^2 s^{-1} at 20°C) or HCO_3^- (1.05×10^{-5} cm^2 s^{-1} at 20°C; Pasciak and Gavis, 1974). The parameters for iCA activity (k_{cf}, k_{cr}) and the mass transfer coefficients for membrane passage ($f_{c\text{-}M}$, $f_{b\text{-}M}$) were determined from analysis of ^{18}O-exchange rates in the presence of an eCA inhibitor (Tu et al., 1978; Hopkinson et al., 2011). eCA-catalyzed hydration/dehydration rate constants (k_{sf}, k_{sr}) are related to each other via the CO_2/HCO_3^- equilibrium constant, assuming microscopic reversibility. k_{sf}, the first-order rate constant for eCA-catalyzed CO_2 hydration, was determined by optimizing the model fit to the ^{18}O-CO_2 data (Supplemental Data S1).

Models of Surface Boundary-Layer Chemistry

To assess the effects of eCA on boundary-layer chemistry, we developed a simple analytical approximation and a one-dimensional numerical reaction diffusion model. The analytical model treats the case in which there is a net CO_2 influx (photosynthetic uptake) to, or efflux (leakage) from, the cell. A net CO_2 influx (an efflux is similar except for a change of sign) is supported by diffusion of CO_2 from the bulk solution and, when eCA is present, the net generation of CO_2 from eCA-catalyzed HCO_3^- dehydration. Diffusion through the boundary layer is dependent on the CO_2 gradient between the bulk solution and the cell surface. For a spherical cell, the net diffusive CO_2 flux (NC_D) is:

$$NC_D = 4\pi RD([CO_2]_e - [CO_2]_s) = f_{c-BL}([CO_2]_e - [CO_2]_s) \quad (8)$$

The net generation of CO_2 from HCO_3^- dehydration at the cell surface is:

$$NC_{eCA} = -k_{sf}[CO_2]_s + k_{sr}[HCO_3^-]_s \quad (9)$$

In the marine environment, which our assay and culture conditions replicate, HCO_3^- concentrations are high, approximately 1.8 mM, and so are not significantly depleted at the cell surface. Taking the HCO_3^- concentration at the surface to be equal to the bulk solution, and using the fact that at equilibrium the forward and backward reaction rates will be equal ($k_{sf}[CO_2] = k_{sr}[HCO_3^-]$), Equation 9 can be rewritten as:

$$NC_{eCA} = k_{sf}([CO_2]_e - [CO_2]_s) \quad (10)$$

In effect, the net CO_2 supply from eCA depends on the same CO_2 gradient as the diffusive supply, although the physicochemical processes underlying these net CO_2 sources are very different. The diffusive flux is driven by the actual spatial CO_2 gradient, whereas net CO_2 production by eCA is the result of disequilibrium between CO_2 and HCO_3^- at the cell surface. The total net CO_2 influx is the sum of the diffusive and reactive supply:

$$NC = (f_{c-BL} + k_{sf})([CO_2]_e - [CO_2]_s) \quad (11)$$

This equation shows that the importance of diffusion or eCA activity for net CO_2 supply depends on the relative sizes of $f_{c\text{-}BL}$ and k_{sf}, justifying k_{sf} as a measure of eCA activity.

Rearranging Equation 11, we can find an expression for the surface CO_2 concentration:

$$[CO_2]_s = [CO_2]_e - \frac{NC}{f_{c-BL} + k_{sf}} \quad (12)$$

which shows that as eCA activity (k_{sf}) increases, the surface CO_2 concentration approaches that of the bulk solution. To measure the impact of eCA on CO_2 exchange between the cell and the bulk solution, we define the effectiveness of eCA (E) as:

$$E = \frac{k_{sf}}{f_{c-BL} + k_{sf}} \quad (13)$$

which varies between 0 (no impact of eCA) and 1 (eCA dominates over diffusive exchange). E is both the fraction of net CO_2 supply supported by eCA and the fraction of the maximum potential CO_2 gradient abolished by eCA activity.

For a more detailed evaluation of the effect of eCA on boundary-layer carbon chemistry and pH, a spherical reaction-diffusion model was developed. The model domain extends from the cell surface 100 μm out to the bulk solution. Chemical concentrations are held constant in the bulk solution but are allowed to vary at the cell surface due to imposed uptake and export fluxes and reaction-diffusion within the boundary layer. Dissolved C_i species (CO_2, HCO_3^-, and CO_3^{2-}) and other important components determining seawater pH [H^+, OH^-, $B(OH)_3$, and $B(OH)_4^-$] are included in the model. Bulk solution pH, C_i, and total boron were set at typical oceanic values (pH 8.14; C_i, 2 mM; total boron, 415 μM). All reactions are treated kinetically using rate constants from Zeebe and Wolf-Gladrow (2001) and diffusion coefficients from Boudreau (1997). The model was solved in Matlab.

Supplemental Data

The following materials are available in the online version of this article.

Supplemental Data S1. Description of scripts used to process isotope exchange data and implement the eCA box model.

ACKNOWLEDGMENTS

We thank François Morel (Princeton University) for helpful advice and discussions.

Received March 12, 2013; accepted May 7, 2013; published May 8, 2013.

LITERATURE CITED

Badger MR (2003) The roles of carbonic anhydrases in photosynthetic CO_2 concentrating mechanisms. Photosynth Res **77:** 83–94

Badger MR, Andrews TJ, Whitney SM, Ludwig M, Yellowlees DC, Leggat W, Price GD (1998) The diversity and coevolution of Rubisco, plastids, pyrenoids, and chloroplast-based CO_2-concentrating mechanisms in algae. Can J Bot **76:** 1052–1071

Badger MR, Palmqvist K, Yu J (1994) Measurement of CO_2 and HCO_3^- fluxes in cyanobacteria and microalgae during steady-state photosynthesis. Physiol Plant **90:** 529–536

Beckmann K, Messinger J, Badger MR, Wydrzynski T, Hillier W (2009) On-line mass spectrometry: membrane inlet sampling. Photosynth Res **102:** 511–522

Boron WF (2004) Regulation of intracellular pH. Adv Physiol Educ **28:** 160–179

Boudreau BP (1997) Diagenetic Models and Their Implemenation: Modelling Transport and Reactions in Aquatic Sediments. Springer-Verlag, Berlin

Burkhardt S, Amoroso G, Riebesell U, Sültemeyer D (2001) CO_2 and HCO_3^- uptake in marine diatoms acclimated to different CO_2 concentrations. Limnol Oceanogr **46:** 1378–1391

Delacruz J, Mikulski R, Tu C, Li Y, Wang H, Shiverick KT, Frost SC, Horenstein NA, Silverman DN (2010) Detecting extracellular carbonic anhydrase activity using membrane inlet mass spectrometry. Anal Biochem **403:** 74–78

Dickson AG, Goyet C, editors (1994) DOE Handbook of Methods for the Analysis of the Various Parameters of the Carbon Dioxide System in Sea Water, Version 2. US Department of Energy, Washington, DC, ORNL/CDIAC-74

Elzenga JTM, Prins HBA, Stefels J (2000) The role of extracellular carbonic anhydrase activity in inorganic carbon utilization of *Phaeocystis globosa* (Prymnesiophyceae): a comparison with other marine algae using the isotopic disequilibrium technique. Limnol Oceanogr **45:** 372–380

Giordano M, Beardall J, Raven JA (2005) CO_2 concentrating mechanisms in algae: mechanisms, environmental modulation, and evolution. Annu Rev Plant Biol **56:** 99–131

Harrison PJ, Waters RE, Taylor FJR (1980) A broad spectrum artificial seawater medium for coastal and open ocean phytoplankton. J Phycol **16:** 28–35

Hopkinson BM, Dupont CL, Allen AE, Morel FMM (2011) Efficiency of the CO_2-concentrating mechanism of diatoms. Proc Natl Acad Sci USA **108:** 3830–3837

Johnson KS (1982) Carbon dioxide hydration and dehydration kinetics in seawater. Limnol Oceanogr **27:** 849–855

Kaplan A, Reinhold L (1999) CO_2 concentrating mechanisms in photosynthetic microorganisms. Annu Rev Plant Physiol Plant Mol Biol **50:** 539–570

Lueker TJ, Dickson AG, Keeling CD (2000) Ocean pCO_2 calculated from dissolved inorganic carbon, alkalinity, and equations for K_1 and K_2: validation based on laboratory measurements of CO_2 in gas and seawater at equilibrium. Mar Chem **70:** 105–119

Martin CL, Tortell PD (2006) Bicarbonate transport and extracellular carbonic anhydrase activity in Bering Sea phytoplankton assemblages: results from isotope disequilibrium experiments. Limnol Oceanogr **51:** 2111–2121

Moroney JV, Husic HD, Tolbert NE (1985) Effect of carbonic anhydrase inhibitors on inorganic carbon accumulation by *Chlamydomonas reinhardtii*. Plant Physiol **79:** 177–183

Moroney JV, Ma YB, Frey WD, Fusilier KA, Pham TT, Simms TA, DiMario RJ, Yang J, Mukherjee B (2011) The carbonic anhydrase isoforms of *Chlamydomonas reinhardtii*: intracellular location, expression, and physiological roles. Photosynth Res **109:** 133–149

Nimer NA, Brownlee C, Merrett MJ (1999) Extracellular carbonic anhydrase facilitates carbon dioxide availability for photosynthesis in the marine dinoflagellate *Prorocentrum micans*. Plant Physiol **120:** 105–112

Nimer NA, Iglesias-Rodriguez MD, Merrett MJ (1997) Bicarbonate utilization by marine phytoplankton species. J Phycol **33:** 625–631

Ohnishi N, Mukherjee B, Tsujikawa T, Yanase M, Nakano H, Moroney JV, Fukuzawa H (2010) Expression of a low CO_2-inducible protein, LCI1, increases inorganic carbon uptake in the green alga *Chlamydomonas reinhardtii*. Plant Cell **22:** 3105–3117

Palmqvist K, Ramazanov Z, Samuelsson G (1990) The role of extracellular carbonic anhydrase for accumulation of inorganic carbon in the green alga *Chlamydomonas reinhardtii*: a comparison between wild-type and cell wall-less mutant cells. Physiol Plant **80:** 267–276

Palmqvist K, Yu JW, Badger MR (1994) Carbonic anhydrase activity and inorganic carbon fluxes in low-C_i and high C_i cells of *Chlamydomonas reinhardtii* and *Scenedesmus obliquus*. Physiol Plant **90:** 537–547

Pasciak WJ, Gavis J (1974) Transport limitation of nutrient uptake in phytoplankton. Limnol Oceanogr **19:** 881–898

Price NM, Harrison GI, Hering JG, Hudson RJ, Nirel PMV, Palenik B, Morel FMM (1988) Preparation and chemistry of the artificial algal culture medium Aquil. Biol Oceanogr **6:** 443–462

Riebesell U, Wolfgladrow DA, Smetacek V (1993) Carbon dioxide limitation of marine phytoplankton growth rates. Nature **361:** 249–251

Rost B, Riebesell U, Burkhardt S, Sültemeyer D (2003) Carbon acquisition of bloom-forming marine phytoplankton. Limnol Oceanogr **48:** 55–67

Silverman D, Lindskog S (1988) The catalytic mechanism of carbonic anhydrase: implications of a rate-limiting protolysis of water. Acc Chem Res **21:** 30–36

Silverman DN (1982) Carbonic anhydrase: oxygen-18 exchange catalyzed by an enzyme with rate-contributing proton-transfer steps. Methods Enzymol **87:** 732–752

Silverman DN, Tu C, Wynns GC (1976) Depletion of ^{18}O from $C^{18}O_2$ in erythrocyte suspensions: the permeability of the erythrocyte membrane to CO_2. J Biol Chem **251:** 4428–4435

Silverman DN, Tu CK, Roessler N (1981) Diffusion-limited exchange of ^{18}O between CO_2 and water in red cell suspensions. Respir Physiol **44:** 285–298

Stewart PS (2003) Diffusion in biofilms. J Bacteriol **185:** 1485–1491

Swietach P, Hulikova A, Vaughan-Jones RD, Harris AL (2010) New insights into the physiological role of carbonic anhydrase IX in tumour pH regulation. Oncogene **29:** 6509–6521

Tilman D (1977) Resource competition between planktonic algae: an experimental and theoretical approach. Ecology **58:** 338–348

Trimborn S, Lundholm N, Thoms S, Richter KU, Krock B, Hansen PJ, Rost B (2008) Inorganic carbon acquisition in potentially toxic and non-toxic diatoms: the effect of pH-induced changes in seawater carbonate chemistry. Physiol Plant **133:** 92–105

Trimborn S, Wolf-Gladrow D, Richter KU, Rost B (2009) The effect of pCO_2 on carbon acquisition and intracellular assimilation in four marine diatoms. J Exp Mar Biol Ecol **376:** 26–36

Tu C, Wynns GC, McMurray RE, Silverman DN (1978) CO_2 kinetics in red cell suspensions measured by ^{18}O exchange. J Biol Chem **253:** 8178–8184

Van K, Spalding MH (1999) Periplasmic carbonic anhydrase structural gene (*Cah1*) mutant in *Chlamydomonas reinhardtii*. Plant Physiol **120:** 757–764

Wolf-Gladrow D, Riebesell U (1997) Diffusion and reactions in the vicinity of plankton: a refined model for inorganic carbon transport. Mar Chem **59:** 17–34

Yoshioka S, Taniguchi F, Miura K, Inoue T, Yamano T, Fukuzawa H (2004) The novel Myb transcription factor LCR1 regulates the CO_2-responsive gene *Cah1*, encoding a periplasmic carbonic anhydrase in *Chlamydomonas reinhardtii*. Plant Cell **16:** 1466–1477

Zeebe RE, Wolf-Gladrow D (2001) CO_2 in Seawater: Equilibrium, Kinetics, Isotopes. Elsevier, Amsterdam

Zhang HN, Byrne RH (1996) Spectrophotometric pH measurements of surface seawater at in-situ conditions: absorbance and protonation behavior of thymol blue. Mar Chem **52:** 17–25